Journal of Nuclear Materials 393 (2009) 203–211

Contents lists available at ScienceDirect

Journal of Nuclear Materials

journal homepage: www.elsevier.com/locate/jnucmat

The effect of processing on the thermal diffusivity of $MgO–Nd_2Zr_2O_7$ composites for inert matrix materials

S.J. Yates [a,b,*], K.J. McClellan [b], J.C. Nino [a]

[a] Department of Materials Science and Engineering, University of Florida, Gainesville, FL 32611, USA
[b] Los Alamos National Laboratory, Los Alamos, NM 87545, USA

ARTICLE INFO

Article history:
Received 20 January 2009
Accepted 3 June 2009

PACS:
28.52.Fa

ABSTRACT

Oxides possess many of the required properties suitable for an inert matrix fuel in light water reactors, however, their primary disadvantage is low thermal conductivity. Composites are being investigated to maximize the thermal conductivity of the inert matrix fuel by using thermally conductive MgO as the primary phase while improving its hot water corrosion resistance through the addition of a second phase acting as a hydration barrier. Inert matrix fuel candidate $MgO–Nd_2Zr_2O_7$ composites were synthesized with multiple processing methods, the composite powders were characterized, the resulting microstructures quantitatively analyzed, and the thermal diffusivity of the composites was measured. Among the four processing methods investigated, ball milling and high-energy shaker blending produced the most homogeneous microstructures with a negligible amount of MgO and $Nd_2Zr_2O_7$ heterogeneities. An effect of processing on the properties of the composites manifests as a larger variation in the thermal diffusivity in pellets processed by methods that produce a higher quantity and frequency of MgO and $Nd_2Zr_2O_7$ heterogeneities than in methods that produce negligible amounts of heterogeneities.

1. Introduction

Inert matrix materials are proposed to perform as non-fertile matrices to burn commercial and weapons grade plutonium in light water reactors and act as transmutation targets to burn the minor actinides. Burning excess plutonium and minor actinides in nuclear reactors and accelerators can potentially reduce the accessible inventory of weapons grade plutonium and significantly reduce the quantity of radioactive waste from commercial reactors that will need to be safely stored [1–9]. Inert matrices provide a stable matrix for actinide incineration without producing plutonium during the fuel cycle.

Among other properties, inert matrix fuels must possess high temperature stability, good irradiation behavior, high thermal conductivity, and reactor coolant compatibility [10]. While oxides adequately address most of these requirements, the primary disadvantage of oxide fuels and their composites is their inherent low thermal conductivity when compared to other fuel types. The thermal conductivity of fuels decreases further under irradiation due to the formation of defects and fission products [11]. The low thermal conductivity of oxides results in an increase in the centerline fuel temperature of the fuel, increasing the difficulty in maintaining a safe thermal margin between the centerline fuel temperature and the melting point of the oxide. Since IMFs are intended for use in current reactor design and operation, the potential IMF should possess a thermal conductivity to melting point ratio that meets or exceeds that of UO_2.

MgO is an excellent candidate for an inert matrix due to its high thermal conductivity and good radiation resistance, however its corrosion resistance is poor since MgO will swell and disintegrate in hot water. $MgO–ZrO_2$ composites attempted to improve the hot water corrosion resistance of MgO through the addition of 40, 50, and 60 vol.% ZrO_2 to act as a hydration barrier, and the resulting composites exhibited adequate thermal conductivities of ~6–9 $W\,m^{-1}\,K^{-1}$ at 1273 K [12]. Lutique et al. [13] have reported calculated thermal conductivities for 50 and 70 vol.% $MgO–Nd_2Zr_2O_7$ composites of ~5–7 $W\,m^{-1}\,K^{-1}$ at 1273 K. Pyrochlores are promising composite constituents since they allow a wide substitution of rare earth elements and some actinides, the structure is radiation tolerant, and molecular dynamics simulations have predicted slightly higher thermal conductivities than that of ZrO_2 [14–17]. Neutronic property calculations on an IMF composed of MgO and $Nd_2Zr_2O_7$ indicated that the best ratio of the phases to provide enough end-of-life reactivity was 7:3 [18].

There is no consistency among researchers in how candidate composite IMF are processed [19–23]. The inconsistencies in composite processing produce considerable variations in the composite

* Corresponding author. Address: Department of Materials Science and Engineering, University of Florida, Gainesville, FL 32611, USA. Tel.: +1 352 846 3768; fax: +1 352 846 3355.
E-mail addresses: sjdyates@yahoo.com, mantha@ufl.edu (S.J. Yates).

0022-3115/$ - see front matter © 2009 Elsevier B.V. All rights reserved.
doi:10.1016/j.jnucmat.2009.06.006

microstructure. Little attention has been given to analyze how the composite microstructures affect the effective properties of these composites. Since thermal transport is sensitive to the microstructure, this paper discusses the effect of processing on the thermal diffusivity of the 70 vol.% MgO–30 vol.% $Nd_2Zr_2O_7$ composite. To determine how the composite processing affects the thermal diffusivity of the composite, this paper characterizes the mixed composite powders from four different composite processing methods, measures the thermal diffusivity of the resulting composites, and associates the effect of processing with the thermal diffusivity of the composites. Future publications will describe the effect of processing on the thermal conductivity of the composites.

2. Experimental procedure

2.1. Composite synthesis

2.1.1. Solid state synthesis of $Nd_2Zr_2O_7$

Stoichiometric ratios of Nd_2O_3 (Alfa Aesar 99.9%) and ZrO_2 (Alfa Aesar 99.7%) were added to spherical 3 and 10 mm yttria stabilized zirconia (YSZ) milling media in a PTFE (polytetrafluoroethylene) ball mill jar with 100 mL of deionized water and 3 mL of ammonium polyacrylate dispersant (20 vol.% Darvan 821A in deionized water). The slurry was milled for 24 h on the ball mill and dried overnight in an oven at 393 K. The dried powder was ground with a porcelain mortar and pestle and sieved through a 212 μm mesh. The sieved powder was placed in an alumina crucible and calcined at 1623 K in air for 12 h. X-ray diffraction (XRD, Philips 3720, Westborough, MA) was performed to verify phase purity. After phase purity was confirmed, a slurry was prepared with the $Nd_2Zr_2O_7$ following the procedure above and re-milled for another 48 h on the ball mill. The powder was dried in an oven at 393 K, ground with the porcelain mortar and pestle, and sieved through the 212 μm mesh.

2.1.2. Mortar and pestle mixing

MgO (Cerac 99.95%) and $Nd_2Zr_2O_7$ were added to an alumina mortar and pestle and ground for 5 min to combine the oxide constituents. The mixed powder was then pressed into pellets and sintered according to the procedure described below.

2.1.3. Magnetic bar stirring

MgO and $Nd_2Zr_2O_7$ were added to a beaker filled with 100 mL of deionized water and 3 mL of ammonium polyacrylate dispersant. The slurry was then stirred with a magnetic bar for 6 h at 200 rpm and dried overnight in an oven at 393 K. The dried powder was ground, sieved, and calcined at 1273 K in air for 2 h before being pressed into pellets.

2.1.4. High-energy shaker blending

MgO and $Nd_2Zr_2O_7$ were placed into a polystyrene container with two 10 mm PMMA (polymethylmethacrylate) spherical blending media. The container was inserted into a high-energy shaker mill (SPEX 8000 M Mixer/Mill), the powder was blended for 45 min and then pressed into pellets.

2.1.5. Ball milling

MgO and $Nd_2Zr_2O_7$ were added to YSZ milling media in a PTFE milling jar with 100 mL of deionized water and 3 mL of ammonium polyacrylate dispersant. The slurry was milled for 24 h and dried overnight in an oven at 393 K. The dried powder was then ground with a porcelain mortar and pestle and sieved through 212 μm mesh. The sieved powder was placed in an alumina crucible and calcined at 1273 K in air for 2 h before being pressed into pellets.

2.1.6. Pellet fabrication

Cylindrical pellets were fabricated from the mixed powders for microstructure and property characterization. The mixed powders described above were combined with 2 wt% of binder (Celvol 103 Polyvinyl Alcohol in deionized water) and ground in an alumina mortar and pestle until the powder sieved through a 300 μm mesh. The sieved powder was then dried in a 393 K oven for 5 min to evaporate the water. The powder was added to a punch and die set lubricated with synthetic 10 W-30 motor oil and pressed with 68 MPa on a Carver press. The pellet was removed from the die and examined for cracks and surface finish. A geometric green density was calculated, and pellets that exceeded 50% of the theoretical density were then sintered in air at 1823 K for 4 h. The sintered pellets were checked for cracks and surface finish and their densities calculated. The Archimedes density was measured and compared to the theoretical density of the 70 vol.% MgO composite calculated from the rule of mixtures. The pellets were then bonded onto polishing substrates and both sides were ground flat and parallel on a polishing wheel (Struers RotoPol-35, Cleveland, OH) using 180 grit SiC paper.

2.2. Composite characterization

2.2.1. Particle size analysis

A representative sample of the constituent and composite powders synthesized by each of the processing methods was added to DI water and placed in an ultrasonic for 1 min to disperse any soft agglomerates. The dispersed powder was then added to a Beckman Coulter LS13320 (Fullerton, CA) and the particle size distribution was measured using laser light scattering.

2.2.2. Scanning electron microscopy

A latitude pellet section was polished to a 1 μm finish with a series of diamond polishing suspensions ending with a 0.5 μm colloidal silica chemi-mechanical polish. The polished sections were placed in an alumina setter, covered, and thermally etched in air for 30 min at 1450 °C. The thermally etched pellets were coated with carbon and examined in a JEOL 6300FXV scanning electron microscope (Peabody, MA) operated at 8 kV at a working distance of 15 mm.

2.2.3. Thermal diffusivity measurements

Flat and parallel disks (<2% variation in thickness) were coated with colloidal graphite on both sides, placed into graphite sample holders, and positioned in a laser flash (Netzsch LFA 457, Germany) carousel with a graphite standard. The thermal diffusivity was measured under flowing Argon from 373 to 1273 K as the temperature increased. Three thermal diffusivity measurements were performed at 100 K intervals after a 15 min hold and a Cowan [24] correction was applied to each measurement by the Netzsch Proteus software. The thermal diffusivity of the graphite standard was compared to the thermal diffusivity of graphite reported by Touloukian [25] to confirm that the laser flash was performing optimally during the sample run.

2.2.4. Quantitative stereology

The microstructure of the composites is described as MgO and $Nd_2Zr_2O_7$ heterogeneities surrounded by a homogeneous interpenetrating matrix of MgO and $Nd_2Zr_2O_7$ grains. Established quantitative stereology techniques as described in Underwood [26] were used to determine the quantity and frequency of the MgO and $Nd_2Zr_2O_7$ heterogeneities. One side of the synthesized pellets was polished to 9 μm with diamond polishing suspensions and analyzed with an optical microscope using polarized light. A grid composed of 10 vertical and 8 horizontal lines was superimposed on 30 unique images for quantitative analysis of the heterogeneities. The

total lineal length of the grid of the analyzed images was calculated to be 1.107 m and the number of points formed by the intersections of the vertical and horizontal lines was 2400. The volume fraction, V_V, of the MgO and $Nd_2Zr_2O_7$ heterogeneities was determined by counting the number of points formed by the intersections of the vertical and horizontal lines that lay on the phase heterogeneities for each phase and dividing it by the total number of points according to the equation

$$V_V = \frac{P_P}{P}, \tag{2.1}$$

where P_P is the number of points that fell on the phase of interest and P is the total number of points. The number of heterogeneity interceptions per unit length N_L was also calculated according to

$$N_L = \frac{N_i}{L}. \tag{2.2}$$

where N_i is the total number of heterogeneities intercepted of the phase of interest and L is the total lineal length of the grid.

3. Results and discussion

3.1. Composite processing

The calcination optimization of the milled Nd_2O_3 and ZrO_2 reported in a previous publication determined that phase pure pyrochlore forms at 1623 K for 12 h with a lattice parameter of 10.678 ± 0.002 Å and a theoretical density of 6.360 ± 0.001 g cm^{-3} [18]. An SEM image of the re-milled $Nd_2Zr_2O_7$ powder in Fig. 1(a) shows uniformly sized grains with some agglomeration. The calcined MgO in Fig. 1(b) is a combination of angular, acicular, and agglomerated particles.

Particle size analysis was performed on the post-calcination milled $Nd_2Zr_2O_7$ and calcined MgO to determine the initial particle size distribution of the constituent phases. The resulting particle size distribution of the $Nd_2Zr_2O_7$ in Fig. 2(a) is consistent with an optimized ball milling process. The shape of the distribution is symmetrical and narrow, with a mode of 2.8 μm. The average particle size for the $Nd_2Zr_2O_7$ is 2.80 ± 1.40 μm and is calculated based on a Gaussian distribution since the particle size of $Nd_2Zr_2O_7$ is normally distributed. The individual grains of $Nd_2Zr_2O_7$ in Fig. 1(a) are much smaller than 2.8 μm, indicating that the individual grains are incorporated into hard agglomerates with an average particle size of 2.8 μm that remain intact after sonication.

The particle size distribution of the MgO in Fig. 2(b) is bimodal with a mode of 0.3 μm for the smaller peak and 5.9 μm for the larger peak. There is also a prominent shoulder at ~20 μm on the right tail of the MgO distribution. The particle size distribution in Fig. 2(b) corresponds reasonably well with the size of the particles and agglomerates in the SEM image in Fig. 1(b), where the majority of the particles appear to be between 1 and 10 μm with a small fraction of particles appearing to measure between 10 and

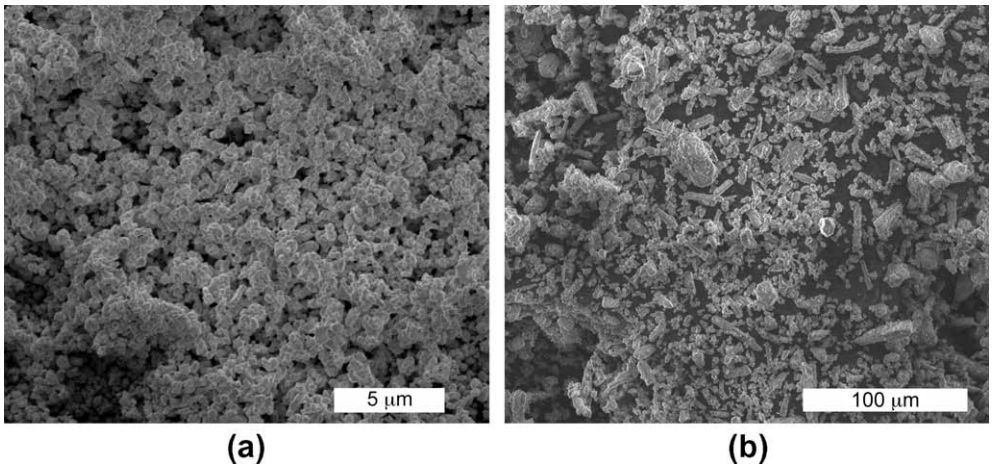

Fig. 1. SEM images of the (a) synthesized $Nd_2Zr_2O_7$ powder and (b) calcined MgO powder.

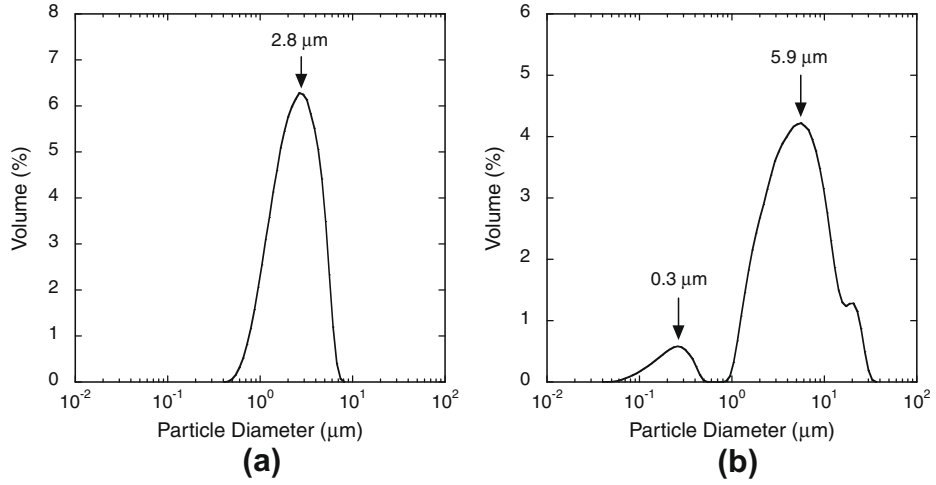

Fig. 2. Particle size distributions for (a) the synthesized $Nd_2Zr_2O_7$ and (b) the calcined MgO powder.

20 μm. Therefore, the MgO powder does not seem to be heavily populated with soft agglomerates because there is no clear difference between the rough visual measurements of the dry powder from Fig. 1(b) and the particle size distribution of the sonicated suspension in Fig. 2(b).

The constituents were combined using four composite processing methods in order to vary the microstructure of the composite to investigate the processing–property relationships. The processing methods employed to synthesize the composites ranged from the crude mortar and pestle mixing of the constituents to an optimized ball milling process. In the case of magnetic bar stirring, the process was transferred from similar work performed on candidate MgO–ZrO_2 IMF composites [21]. The four processing methods can be separated into two distinct categories of dry vs. aqueous processes. As the XRD profiles show in Fig. 3, the dry synthesis methods, mortar and pestle and high-energy shaker

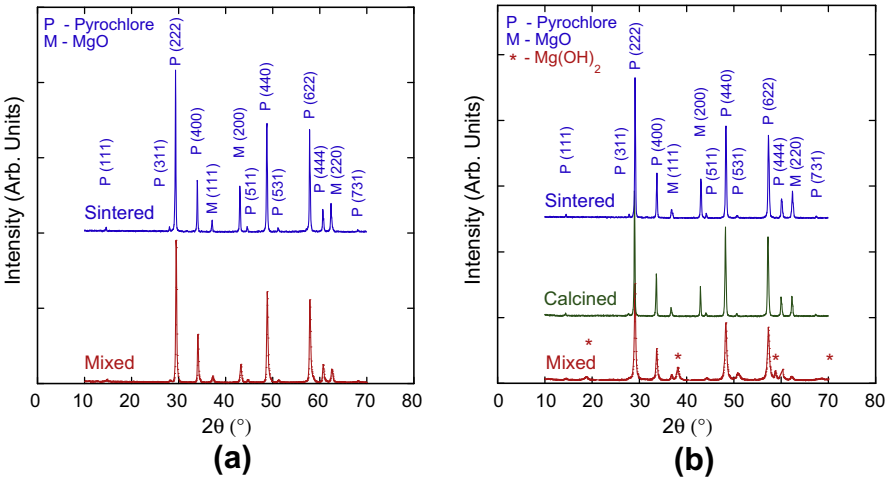

Fig. 3. XRD profiles of mixed and sintered composites from (a) dry processing methods and (b) aqueous processing methods. In the aqueous processes MgO transforms into $Mg(OH)_2$ during mixing requiring an extra calcination step to transform the $Mg(OH)_2$ into MgO before sintering.

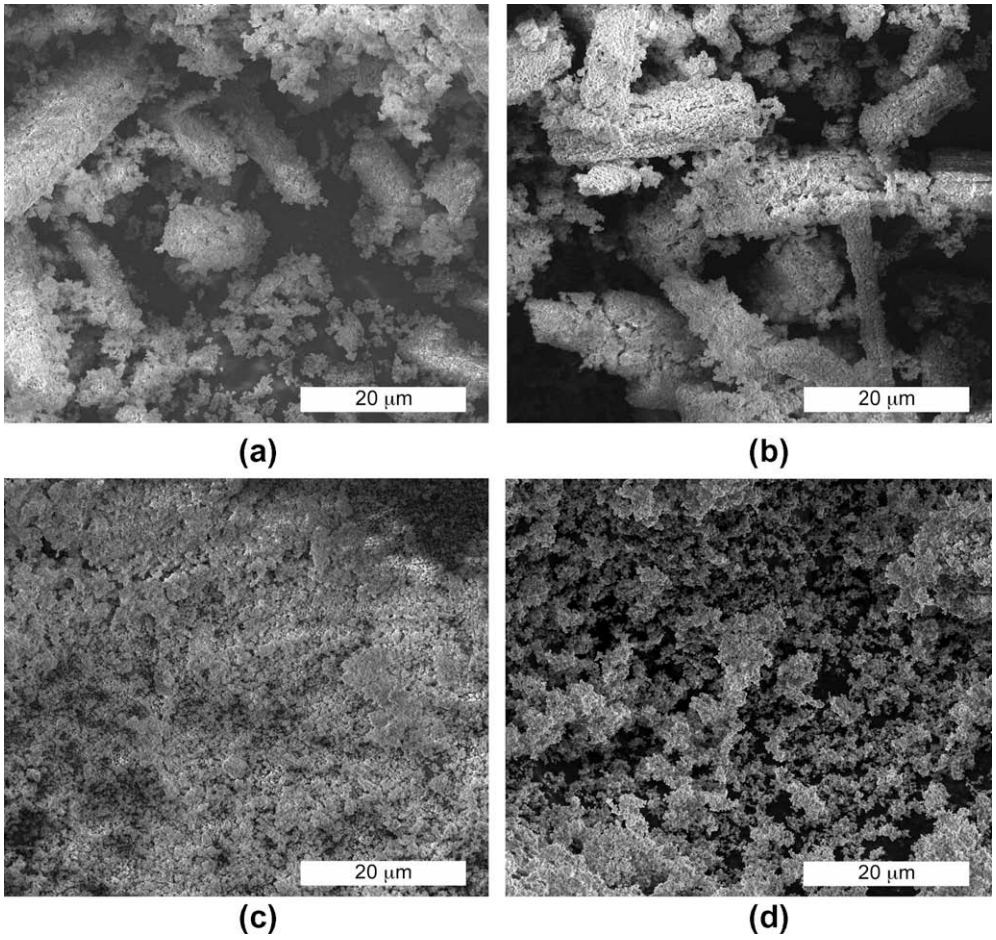

Fig. 4. SEM images of the composite powders synthesized by (a) mortar and pestle, (b) magnetic bar stirring, (c) high-energy shaker blending and (d) ball milling.

blending, generate composite powder composed of only the constituent phases, MgO and $Nd_2Zr_2O_7$, after mixing and sintering. However, the aqueous-based synthesis methods, magnetic bar stirring and ball milling, transform MgO into $Mg(OH)_2$ through a hydration reaction with the deionized water during mixing. In an attempt to mitigate the formation of $Mg(OH)_2$ during mixing alcohol and acetone were also used as ball milling solvents, but XRD of the mixed powder showed that MgO still transformed to $Mg(OH)_2$ in the alcohol and acetone based slurries. The XRD profiles in Fig. 3(b) show that an extra calcination step added after mixing and before sintering in the aqueous processing methods transforms the $Mg(OH)_2$ back into MgO before sintering. A significant advantage of the dry processing methods is the extra calcination step is not necessary and the mixed powder can be immediately pressed into pellets.

SEM images of the mixed composite powders are shown in Fig. 4. It can be immediately observed that there is a difference in the morphology of the mortar and pestle and magnetic bar stirred composite powders in Fig. 4(a) and Fig. 4(b) compared to the high-energy shaker blended and ball milled powder in Fig. 4(c) and (d). In the cases of the mortar and pestle and magnetic bar stirred powder, the mixed powders are composed of large acicular agglomerates while the high-energy shaker blended and ball milled powders are composed of smaller and relatively spherical agglomerates. Particle size analysis was performed on the composite powders and the results are shown in Fig. 5.

The particle size distributions for the mortar and pestle and magnetic bar stirred composite powders are slightly skewed toward the larger particle sizes. Comparing the SEM images of the mortar and pestle and magnetic bar stirred composite powders in Fig. 4(a) and (b) with the results of the particle size distribution in Fig. 5(a) and (b) it can be inferred that the acicular agglomerates are partially weak in character because in the SEM images the acicular agglomerates are mostly over 20 μm in size and in the particle size distribution in Fig. 5(a) and (b) most of the particles are less than 20 μm in size. Therefore, the acicular agglomerates must have partially broken up when suspended and sonicated before particle size analysis was performed.

In the cases of the mortar and pestle and magnetic bar stirring composite powders the modes of the particle sizes are greater than that of either the constituent MgO or $Nd_2Zr_2O_7$. This suggests that hard agglomerates of the constituents formed during the mixing process and are present in the composite powder prior to sintering. There is also a prominent shoulder present at ~20 μm in the particles size distribution of the magnetic bar stirred composite powder, indicating that more hard agglomerates are present in the magnetic bar stirred composite powder than in the mortar and pestle powder. The presence of agglomerates is particularly concerning because they can inhibit composite densification and cause differential sintering [27–29]. Differential sintering can lead to cracking within the composite microstructure. Therefore, powder characterized by a narrow distribution of small particle sizes is

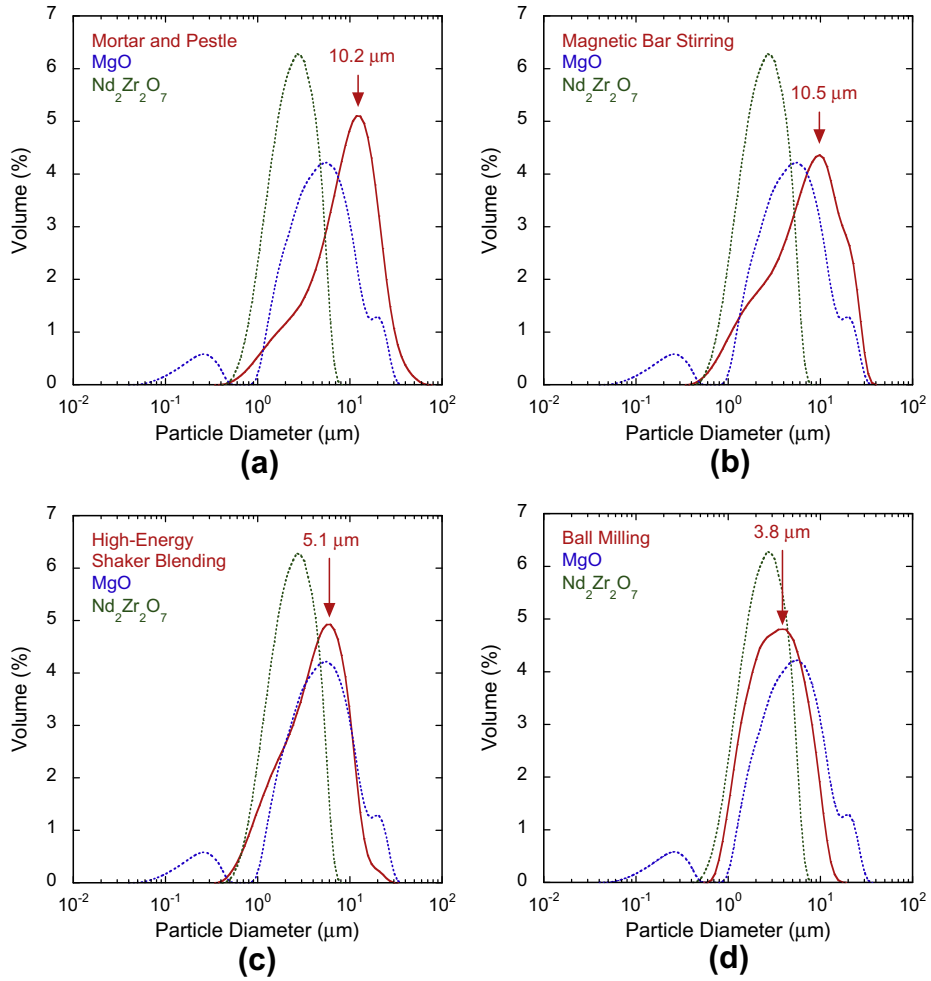

Fig. 5. Particle size distribution of the $Nd_2Zr_2O_7$ and MgO feed stock and synthesized composite powder for (a) mortar and pestle, (b) magnetic bar stirring, (c) high-energy shaker blending and (d) ball milling.

more likely to result in dense composites with a homogeneous microstructure.

Large agglomerates do not form during the mixing of the constituents in high-energy shaker blended and ball milled composites. Although the particle size distribution of the high-energy shaker blended powder in Fig. 5(c) is also shifted toward the larger particle sizes, the mode of the composite powder is only 5.1 μm, similar enough to that of the MgO to suggest there was little or no agglomeration during mixing. In fact, there appears to be a reduction in the number of 20 μm agglomerates in the high-energy shaker blended powder, indicating that high-energy shaker blending imparted enough mechanical energy on the constituents to break up agglomerates present from the MgO powder.

The particle size distribution for the ball milled powder in Fig. 5(d) is normally distributed with an average particle size of 4.2±2.7 μm. Of the four processing methods, ball milling produces a particle size distribution with the smallest mode, smallest average, and is the most normally distributed. This is not an unexpected result since these characteristics are the product of an optimized ball milling process. In addition, all of the 20–50 μm agglomerates have disappeared demonstrating that ball milling the constituents together provides enough mechanical energy to break up the MgO agglomerates from the constituent powder into smaller particles.

Pellets were fabricated and sintered from each batch of synthesized composite powder. Density measurements were performed on three pellets from each batch of composite powder. Pellets fabricated with composite powder synthesized using magnetic bar stirring were measured to be 90% dense, while mortar and pestle pellets were measured to be 96% dense and pellets fabricated from high-energy shaker blending and ball milling were 97% dense based on the Archimedes density. There was only a variation in the measured densities of the pellets of ±0.5% between the pellets from each batch of composite powder, which indicates that pellet densities are relatively consistent. The decrease in sintered density for the magnetic bar stirred composites is most likely due to the presence of hard agglomerates in the composite powder, since variations in particle packing between the matrix and the agglomerates will affect pore evolution during sintering [27].

The microstructures resulting from the mixed composite powders were characterized using optical microscopy. The microstructure can be described as a distribution of MgO and $Nd_2Zr_2O_7$ heterogeneities within an interpenetrating matrix of MgO and $Nd_2Zr_2O_7$ grains. Since reflected polarized light was used, the two phases can be differentiated in the optical images in Fig. 6 due to the difference in their refractive indices. The solid white phase in the optical images is $Nd_2Zr_2O_7$ and the solid black phase is MgO. EDS of the MgO and $Nd_2Zr_2O_7$ heterogeneities shows that there is limited solubility of the MgO in the $Nd_2Zr_2O_7$ and MgO in the $Nd_2Zr_2O_7$. The mottled grey phase surrounding the MgO and $Nd_2Zr_2O_7$ heterogeneities is the homogeneous interpenetrating matrix. Porosity would also appear to be solid black in the optical images, but examination of the composite microstructures with SEM shows that the porosity is only on the order of 3–5 μm and large MgO heterogeneities were present in the composite. Therefore, the dark regions associated with the residual porosity are incorporated into the interpenetrating matrix.

While heterogeneities of MgO and $Nd_2Zr_2O_7$ can be observed in all of the composites, there is clearly a visible difference in the size and frequency of the heterogeneities between the composites syn-

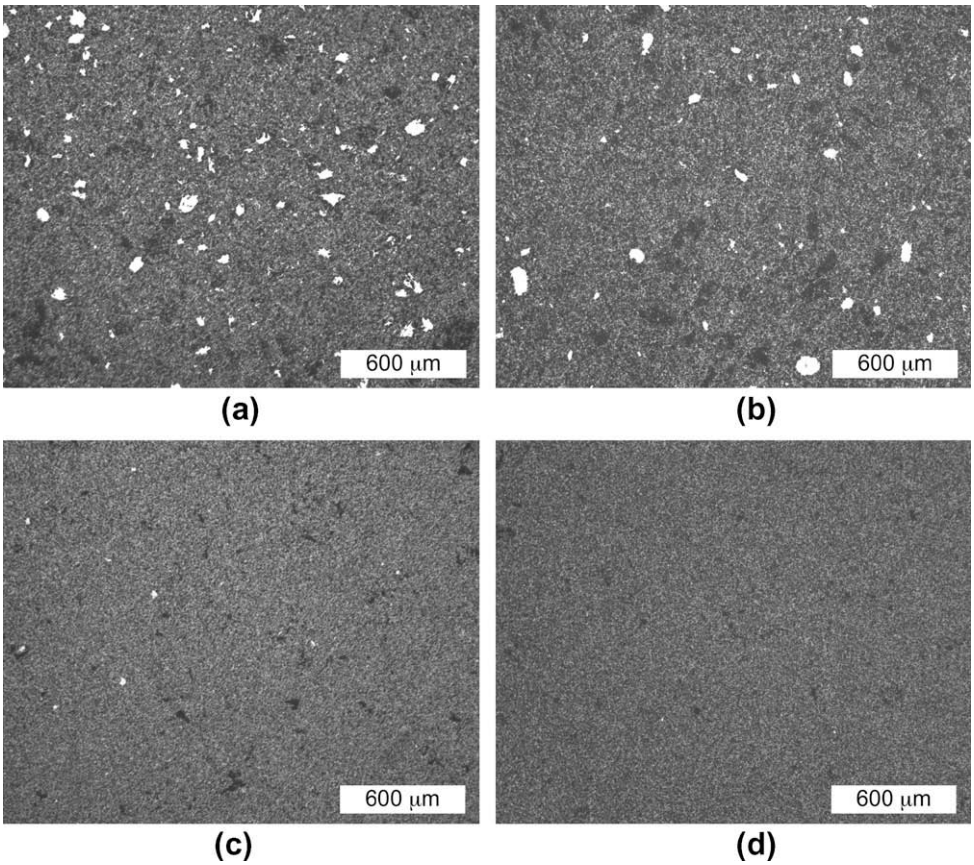

Fig. 6. Optical images of composite microstructures processed by (a) mortar and pestle, (b) magnetic bar stirring, (c) high-energy shaker and (d) ball milling. The MgO heterogeneities are the solid black phase and the $Nd_2Zr_2O_7$ heterogeneities are the solid white phase. The MgO and $Nd_2Zr_2O_7$ heterogeneities are surrounded by the mottled grey interpenetrating matrix.

thesized by high-energy shaker blending and ball milling and those found in the composites synthesized by the mortar and pestle and magnetic bar stirring. When the composite powder is relatively uniform and lightly agglomerated, as in the high-energy shaker blended and ball milled composite powders, the heterogeneities are much smaller and occur less frequently. In the case of the mortar and pestle and magnetic bar stirred composite powders there is a significant population of hard agglomerates in the mixed composite powder. Therefore, it is believed that the agglomerates are the source of the heterogeneities observed in the sintered composites in Fig. 6 since it is unlikely that the green packed agglomerates will rearrange during sintering to homogenize the microstructure.

3.2. Thermal diffusivity

To determine the effect of processing on the thermal diffusivity of the composites, multiple pellets were measured from each batch of mixed composite powder. Three different pellets from each batch of mixed composite powder were measured, the results were compiled, and the best fit to the thermal diffusivity data was calculated. In Fig. 7, a 95% confidence interval has been calculated from the compiled thermal diffusivity measurements. The confidence intervals for the high-energy shaker blended and ball milled composites in Fig. 7(c) and (d) are relatively narrow and approximately the same width. However, the width of the confidence interval in the mortar and pestle composites is approximately twice the width of the ball milled composites and the width of the confident interval in the magnetic bar stirred composites is nearly 4 times the width of the ball milled composites. The wider confidence bands in the mortar and pestle and magnetic bar stirred composites compared to that of high-energy shaker blended or ball milled composites implies that the thermal diffusivity can be predicted less reliably across a population of mortar and pestle and magnetic bar stirred composites than in high-energy shaker blended and ball milled composites.

The relationship between the width of the confidence interval and composite processing was investigated in an attempt to determine the cause of the scatter in the data. The most observable difference between the composites synthesized by mortar and pestle and magnetic bar stirring versus high-energy shaker blending and ball milling is the difference in the quantity and frequency of MgO and $Nd_2Zr_2O_7$ heterogeneities in the sintered composites. Quantitative stereology was used to analyze the MgO and $Nd_2Zr_2O_7$ heterogeneities for each processing method by treating the heterogeneities as second phase particles dispersed in a homogeneous matrix phase. The results are summarized below in Table 1 for the MgO and $Nd_2Zr_2O_7$ heterogeneities, where the volume fraction describes the quantity of the MgO and $Nd_2Zr_2O_7$ heterogeneities and N_L describes the frequency of the heterogeneities. Since the matrix is composed of a homogeneous distribution of interpene-

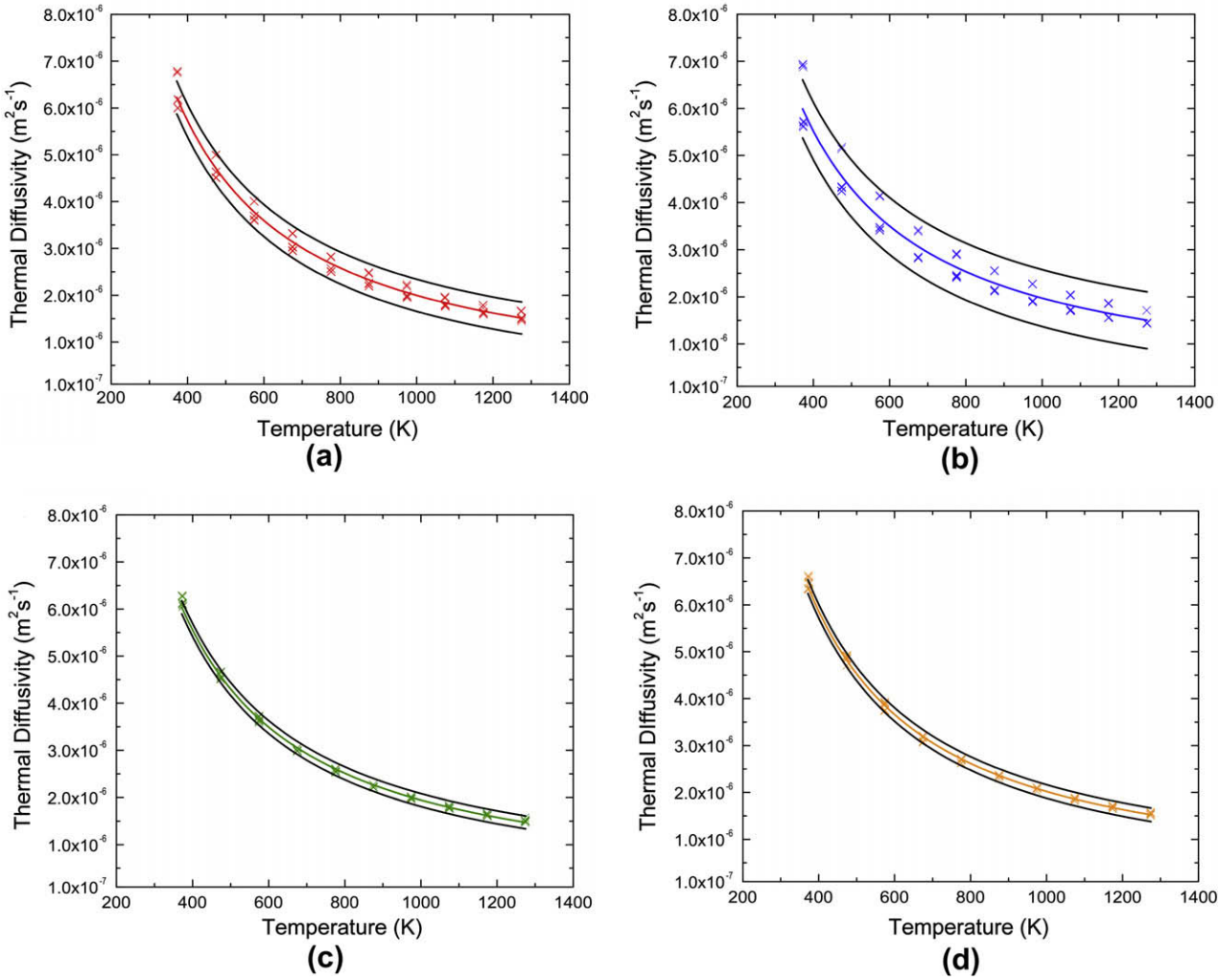

Fig. 7. The thermal diffusivity and corresponding 95% confidence interval of pellets processed by (a) mortar and pestle, (b) magnetic bar stirring, (c) high-energy shaker blending and (d) ball milling.

Table 1
Quantitative stereology results for the quantity and frequency of MgO and $Nd_2Zr_2O_7$ heterogeneities.

Process	MgO		$Nd_2Zr_2O_7$		Total	
	Volume fraction (%)	N_L (m^{-1})	Volume fraction (%)	N_L (m^{-1})	Volume fraction (%)	N_L (m^{-1})
Mortar and pestle	0.29	40	1.92	424	2.21	464
Magnetic bar stirring	1.33	128	0.73	161	2.06	289
High-energy shaker blending	0.13	53	0.04	22	0.17	75
Ball milling	0.40	60	0.04	21	0.44	81

trating MgO and $Nd_2Zr_2O_7$ grains arranged in single phase clusters of 5–10 grains, the heterogeneities that approached the average size of the single phase clusters in the composites were ignored. Therefore, a heterogeneity was defined as a solid cluster of a single phase with a cross-section larger than ~15 μm.

From the stereology data it can be observed that in the case of the mortar and pestle and magnetic bar stirred composites, the total volume fraction of the heterogeneities is much greater than that of the high-energy shaker blended or ball milled composites. The frequency of the MgO and $Nd_2Zr_2O_7$ heterogeneities is also greater in the mortar and pestle and magnetic bar stirred composites than in high-energy shaker blended or ball milled composites. The volume fraction of heterogeneities for the mortar and pestle and magnetic bar stirred composites is nearly the same, and the volume fraction of heterogeneities for the high-energy blended and ball milled composites is relatively low. High-energy shaker blended and ball milled composites are virtually identical in the quantity and frequency of heterogeneities according to the quantitative stereology results, although subtle differences between the composites can be observed in the optical images. No strong correlation between the volume fraction of heterogeneities and the frequency of the heterogeneities is observed. The stereology data supports this conclusion because a small difference in the total volume fraction of the heterogeneities produces a large difference in the frequency of the heterogeneities in the mortar and pestle and magnetic bar stirred composites, and a larger proportional difference in volume fraction of heterogeneities produces a slight difference in the frequency of the heterogeneities in the high-energy shaker blended and ball milled composites. If composite homogeneity is defined as the combination of a small volume fraction and a low frequency of the heterogeneities, then the data in Table 1 can adequately characterize the effect of the processing method on the homogeneity of the composite. By adhering to this criteria and combining it with the results from the particle size analysis, high-energy shaker blending and ball milling produces the most homogeneous microstructures among the four composite processing methods investigated.

Further, a correlation emerges that suggests that the predictability of the thermal diffusivity is related to the presence of MgO and $Nd_2Zr_2O_7$ heterogeneities. The width of the confidence interval is much larger in mortar and pestle and magnetic bar stirred composites than in the high-energy shaker blended and ball milled composites. Particularly in the case of $Nd_2Zr_2O_7$, there is a significant difference between the quantity and frequency of the heterogeneities for the mortar and pestle and magnetic bar stirring composites and those synthesized using high-energy shaker blending and ball milling. In the ball milled and high-energy shaker milled processes where the quantity and frequency of the heterogeneities is small, the confidence interval width is relatively narrow. In the magnetic bar stirring and mortar and pestle processes that possess a large quantity and high frequency of heterogeneities, the width of the confidence interval in the thermal diffusivity measurements is relatively large.

The composite microstructures were analyzed in more detail on polished and thermally etched samples. During the inspection, circumferential cracking characteristic of differential sintering was observed between the heterogeneities and the interpenetrating matrix. Cracks between the heterogeneities and the interpenetrating matrix would be detrimental to the effective conductivity of the composite, and could also be responsible for the variation in the thermal diffusivity of the composites. Representative images of the heterogeneity–matrix interface are shown in Fig. 8. In Fig. 8(a) the heterogeneity–matrix interface is intact, but in Fig. 8(b) circumferential cracking characteristic of differential sintering has occurred between the heterogeneity and matrix. These samples were not thermally shocked, nor is it likely that the differ-

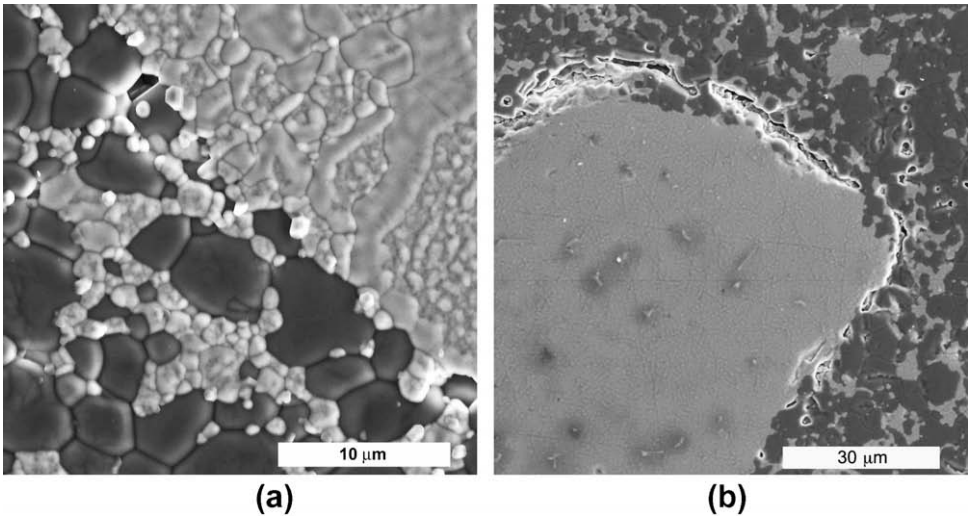

Fig. 8. SEM images of $Nd_2Zr_2O_7$ heterogeneities showing (a) an intact interface between the heterogeneity and the interpenetrating matrix and (b) cracking between the heterogeneity and the interpenetrating matrix.

ence between the coefficient of thermal expansion of the $Nd_2Zr_2O_7$ and interpenetrating matrix is extreme enough to cause catastrophic stresses to build between the heterogeneity and the matrix. Therefore, the cracking between the heterogeneity and the interpenetrating matrix is probably not caused by thermal expansion mismatch. Cracks were not observed in either high-energy shaker blended or ball milled composites, however cracks between the heterogeneity–interpenetrating matrix interface were found in both mortar and pestle and magnetic bar stirring composites. Although the interface was intact in most of the heterogeneities randomly inspected across the mortar and pestle and magnetic bar stirring composites, cracks between the heterogeneity–matrix interface did appear regularly during the survey of the composites. The cracking was found between $Nd_2Zr_2O_7$ heterogeneities and the interpenetrating matrix, and nearly but not always near the relatively large $Nd_2Zr_2O_7$ heterogeneities.

The correlation between the frequency and distribution of the $Nd_2Zr_2O_7$ heterogeneities and the standard deviation of the thermal diffusivity is most likely due to the formation of these circumferential cracks between the heterogeneity–interpenetrating matrix interface. The hard agglomerates present in the mortar and pestle and magnetic bar stirred composite powders are composed of loosely packed particles connected by solid chemical bridges of material. The density of these loosely packed agglomerates is lower than the density of the surrounding matrix, and the difference between the green density of the hard agglomerate and the matrix causes strains to develop during sintering as the hard agglomerates densifies faster than the surrounding matrix [30]. When these stresses that arise due to these strains exceed that of the interfacial bond between the agglomerate and the matrix, a circumferential crack is formed. Since the magnetic bar stirred composite powder contained more hard agglomerates than the mortar and pestle powder, the density of circumferential cracks is expected to be higher in the magnetic bar stirred composites than in the mortar and pestle composites. The effective thermal diffusivity of the composites would then be expected vary across a population of samples because some samples may contain more or less cracking than others [31,32]. Therefore, the width of the confidence interval in the magnetic bar stirred composites is larger because there is a higher density of circumferential cracks compared to that of the mortar and pestle composites.

4. Conclusions

Candidate IMF 70 vol.% MgO–30 vol.% $Nd_2Zr_2O_7$ composites were synthesized by four different processing methods. The mixed composite powder was characterized for each processing method, the resulting microstructures were characterized, and thermal diffusivity was measured from 373 to 1273 K. In the four processing methods investigated, mortar and pestle and magnetic bar stirring produce composites with a larger quantity and higher frequency of MgO and $Nd_2Zr_2O_7$ heterogeneities than high-energy shaker blended or ball milled composites. High-energy shaker blending and ball milling produce nearly homogeneous composites with a negligible amount of heterogeneities within the microstructure. Quantitative stereology established a relationship between the presence of hard agglomerates in the mortar and pestle and magnetic bar stirring composite powder and the presence of heterogeneities in the sintered composites. As expected, the composite microstructure affects the thermal diffusivity. The increase in the quantity and frequency of the heterogeneities in the mortar and pestle and magnetic bar stirring composites decreases the predictability of the thermal diffusivity of the composites. The increase in the variability in the thermal diffusivity is most likely due to the presence of circumferential cracking around $Nd_2Zr_2O_7$ heterogeneities. The circumferential cracks between the heterogeneities and interpenetrating matrix are likely caused by differential sintering originating from the presence of hard agglomerates in the mixed composite powders. Although the scatter in the thermal diffusivity data can be correlated with the presence of heterogeneities in the composite microstructures, they do not correspond with the trend observed in the overall thermal conductivity of the composites. Further work is focused on the characterization of the interpenetrating matrix in order to analyze how processing affects the thermal conductivity of the composites.

Acknowledgements

The authors would like to thank the Department of Energy for their support of this project under the Nuclear Energy Research Initiative (NERI) award DE-FC07 – 51D14647 and the Global Nuclear Energy Partnership (AFCI).

References

[1] C. Degueldre, J.M. Paratte, J. Nucl. Mater. 274 (1999) 1.
[2] G. Ledergerber, C. Degueldre, P. Heimgartner, M.A. Pouchon, U. Kasemeyer, Prog. Nucl. Energy 38 (2001) 301.
[3] V.M. Oversby, C.C. McPheeters, C. Degueldre, J.M. Paratte, J. Nucl. Mater. 245 (1997) 17.
[4] K.E. Sickafus, R.J. Hanrahan, K.J. McClellan, J.N. Mitchell, C.J. Wettel, D.P. Butt, P. Chodak, K.B. Ramsey, T.H. Blair, K. Chidester, H. Matzke, K. Yasuda, R.A. Verrall, N. Yu, Am. Ceram. Soc. Bull. 78 (1999) 69.
[5] A.V. Vatulin, Y.A. Stetsky, Y.I. Trifonov, G.I. Khotyashov, Prog. Nucl. Energy 38 (2001) 321.
[6] L.C. Walters, D.L. Porter, D.C. Crawford, Prog. Nucl. Energy 40 (2002) 513.
[7] T. Yamashita, K. Kuramoto, H. Akie, Y. Nakano, N. Nitani, T. Nakamura, K. Kusagaya, T. Ohmichi, J. Nucl. Sci. Tech. 39 (2002) 865.
[8] M. Osaka, H. Serizawa, M. Kato, K. Nakajima, Y. Tachi, R. Kitamura, S. Miwa, T. Iwai, K. Tanaka, M. Inoue, Y. Arai, J. Nucl. Sci. Technol. 44 (2007) 309.
[9] R.J.M. Konings, D. Haas, C. R. Phys. 3 (2002) 1013.
[10] H. Matzke, V.V. Rondinella, T. Wiss, J. Nucl. Mater. 274 (1999) 47.
[11] S.G.C. Popov, J.J. Ivanov, V.K. Yoder, Oak Ridge National Laboratory, ORNL/TM-2000/351.
[12] P.G. Medvedev, M.J. Lambregts, M.K. Meyer, J. Nucl. Mater. 349 (2006) 167.
[13] S. Lutique, R.J.M. Konings, V.V. Rondinella, J. Somers, T. Wiss, J. Alloy. Compd. 352 (2003) 1.
[14] M.A. Subramanian, G. Aravamudan, G.V.S. Rao, Prog. Solid State Chem. 15 (1983) 55.
[15] K.E. Sickafus, L. Minervini, R.W. Grimes, J.A. Valdez, M. Ishimaru, F. Li, K.J. McClellan, T. Hartmann, Science 289 (2000) 748.
[16] P.K. Schelling, S.R. Phillpot, R.W. Grimes, Phil. Mag. Lett. 84 (2004) 127.
[17] R.C. Ewing, W.J. Weber, J. Lian, J. Appl. Phys. 95 (2004) 5949.
[18] S.J. Yates, P. Xu, J. Wang, J.S. Tulenko, J.C. Nino, J. Nucl. Mater. 362 (2007) 336.
[19] K. Bakker, R.J.M. Konings, J. Nucl. Mater. 254 (1998) 129.
[20] Y.W. Lee, H.S. Kim, S.H. Kim, C.Y. Joung, S.H. Na, G. Ledergerber, P. Heimgartner, M. Pouchon, M. Burghartz, J. Nucl. Mater. 274 (1999) 7.
[21] P.G. Medvedev, J.F. Jue, S.M. Frank, M.K. Meyer, J. Nucl. Mater. 352 (2006) 318.
[22] S. Pillon, J. Somers, S. Grandjean, J. Lacquement, J. Nucl. Mater. 320 (2003) 36.
[23] R.P.C. Schram, R.R. van der Laan, F.C. Klaassen, K. Bakker, T. Yamashita, F. Ingold, J. Nucl. Mater. 319 (2003) 118.
[24] R.D. Cowan, J. Appl. Phys. 34 (1963) 926.
[25] Y.S. Touloukian, E.H. Buyco, Specific Heat: Nonmetallic Solids, Plenum, New York, 1970.
[26] E.E. Underwood, Quantitative Stereology, Addison-Wesley, Reading, MA, 1970.
[27] F.F. Lange, J. Am. Ceram. Soc. 67 (1984) 83.
[28] M.N. Rahaman, Ceramic Processing and Sintering, Marcel Dekker Inc., New York, NY, 2003.
[29] A.G. Evans, J. Am. Ceram. Soc. 65 (1982) 497.
[30] F.F. Lange, M. Metcalf, J. Am. Ceram. Soc. 66 (1983) 398.
[31] D.P.H. Hasselman, J. Compos. Mater. 12 (1978) 403.
[32] A. Hoenig, J. Compos. Mater. 17 (1983) 231.